

A Review of Microcolorimetry for Textile, Food, Dental and Optoelectronic Industries

H. J. Swatland

University of Guelph,

Guelph, Canada

Email: swatland [AT] uoguelph.ca

ABSTRACT--- *A microscope spectrophotometer may be used for colorimetry with transmitted, reflected or emitted light. Optical fibers may be used to link the microscope to remote samples, which may be commercial color standards like Pantone or paint manufacturers' color chips, or small museum specimens. The weighted-ordinate method of colorimetry gives useful results for a wide variety of samples, although light scattering in small samples like textile fibers has some important effects that may be missed in macroscopic colorimetry. The weighted-ordinate method is applicable to metallic and pastel interference colors, with printed simulations and real interference colors giving similar results. Thus, spectrophotometry is still required to identify fake security holograms. Some classic work was confirmed, showing how immersion under water may be used to identify a source of iridescence. Multilayer interference in molluscan shell nacre had multiple spectral peaks easily detectable under water, whereas diffractive interference on a peacock feather had a single spectral peak lost under water. Iridescence in single muscle fibers from roast meat resembled multilayer interference in having multiple spectral peaks that were easily visible under water, and the importance of optical anisotropy in food colorimetry was considered. Boolean analysis of fiber-optic spectra may be used instead of the weighted-ordinate method for spectra obtained robotically in a contextual learning mode. From investigating museum samples to quality control using optoelectronic components, microcolorimetry may have a promising future.*

Keywords--- Microscopy, Fiber optics, Weighted-ordinate colorimetry, Interference colors, Iridescence

1. INTRODUCTION

Macroscopic colorimetry has been essential in quality control at the interface of manufactured goods with consumers for decades, everything from the colors of foods, to matching the colors of interior plastics with the outside paint on automobiles. White bathroom ceramics and printer papers have proved challenging, as whiteners and the emission spectra of common household light sources have evolved, but industrial colorimetry has answered the challenge [1]. But now we are looking at much smaller areas, from pixels on display screens, to machine vision of medical biopsy sections, so this could be the advent of microcolorimetry. Thus, it is reasonable to consider the background to this fascinating subject.

The microscopic study of color goes back a long way, to the year 1665 with Robert Hooke's great work *Micrographia* [2], where he explained how surface diffraction on peacock feathers causes iridescence. His observation that diffraction colors are lost under water is still useful today in the investigation of contentious topics, such as iridescence on meat and fish muscle, as will be demonstrated later in this review. Firstly, however, it is necessary to consider how microscopy and fiber optics may be used – there are countless possibilities, but the data reported here are inadequate without knowing how they were collected. With microscopy and fiber optics, it is difficult, if not impossible, to attain the standards of agreement and transferability reached by the CIE system (Commission International de l'Éclairage) with tightly controlled aperture sizes, angles of illumination, and illumination emission spectra [1]. However, the weighted-ordinate method of colorimetry basic to the CIE system is surprisingly robust, and generates chromaticity coordinates that agree subjectively with positions in the CIE color chart. This review looks at difficult problems in microcolorimetry because they pose a greater challenge than routine quality control measurements.

2. APPARATUS

A microscope is a great tool for microcolorimetry, it may focus directly on very small structures, or focus on optical fibers connected to a sample (Figure 1). Optical plans and programming algorithms are available [3]. It may use a grating monochromator (Figure 1, 3) with stray-light filters to remove unwanted harmonics (Figure 1,2), but there are other possibilities, such as a diode-array spectrograph. A monochromator scanned from 400 to 700 nm in steps of 10 nm with a 10 nm band-pass is adequate for most colorimetry applications. An illuminator is needed, with a 100 W halogen source operated from a stabilized power supply (Figure 1,14) being a conventional but not irreplaceable source. A solenoid shutter (Figure 1, 13) is needed (to correct for dark-field illumination) plus a vertical illuminator with a beam splitter (Figure 1,6) to illuminate samples or optical fibers. The microscope objectives should be corrected for reflected light

with no cover slip (Figure 1, 7), but this is seldom critical. For transmitted light, beneath the sample stage (Figure 1, 8) a condenser is needed (Figure 1, 9). Mirrors may be used to switch from transmitted to reflected light (Figure 1; 10, 11 and 15). For transmitted light, the system is best standardized on a clear area to one side the specimen, with the polarizer (Figure 1, 12) parallel to the analyzer (Figure 1, 4) and a tilting compensator set at 0° (Figure 1, 5). A tilting compensator (Figure 1,5) for generating interference colors with transmitted light is most useful. As discussed later, results reported here are relative to the diffuse reflectance of several layers of Teflon tape (polytetrafluoroethylene [4]), but other standards might be possible. When working on interference colors, fractions of the dynamic range of the photometer might be needed, because the intensity of constructive interference at certain wavelengths may exceed that of a standard for diffuse illumination.

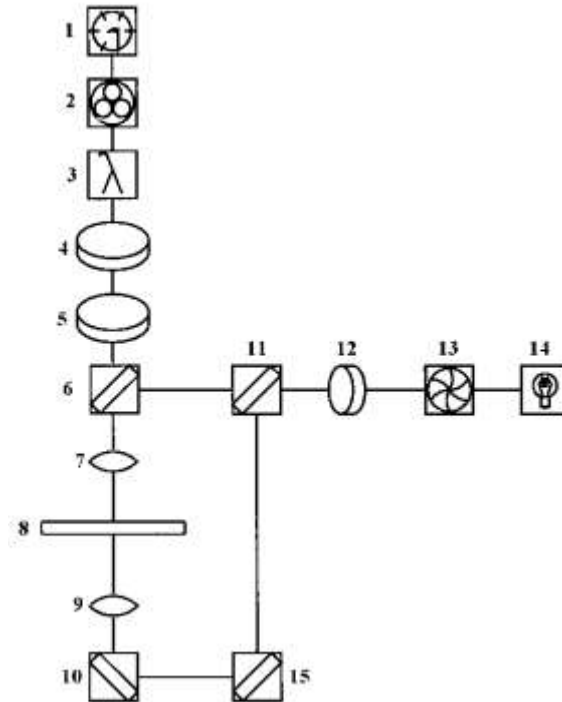


Figure 1. Optical plan showing photomultiplier (1), stray-light filter (2), grating monochromator (3), analyzer (4), tilting compensator (5), beam splitter (6), objective (7), sample stage (8), substage condenser (9), fixed mirror (10), slide-in mirror (11), polarizer (12), solenoid shutter (13), halogen illuminator (14) and fixed mirror (15).

For fiber optics, swing-in mirrors between components 12 and 13, and between 3 and 4 in Figure 1 may be used. This enables illumination to be directed into one branch of a bifurcated fiber-optic probe, while light returned from the probe returns through the spectrophotometer. For the data shown here, the probe had six illuminating fibers in a ring around a central receiving fiber – but different configurations give different results, especially when in direct contact with translucent specimens. Thus, a light guide with two D-shaped back-to-back groups of optical fibers forces a light path through the sample with selective absorbance dominating over light scattering, while a random arrangement of illuminating and receiving fibers responds more to scattering than to selective absorbance. Another factor influencing fiber optic colorimetry is the nature of the interface between the optical fibers and the specimen. For a hard specimen with minimal translucence, there is bound to be an air space at the interface, either very small and uncontrolled, or large and controlled by the extent that the optical fiber is backed away from the specimen. Depending on the numerical apertures of optical fibers, the interface may produce chromatic aberration and, thus, should be controlled to match the conditions established at the time of standardization. As may be shown by total internal reflection back up an illuminating fiber, the refractive index of the medium beyond a fiber and the angle of the end window in the fiber also have a chromatic effect [5]. Strictly speaking, fiber-optic reflectance is sterance or solid-angle flux measured per unit area.

3. PIGMENTS IN TEXTILES AND MUSEUM EXHIBITS

Macroscopic colorimetry is widely used in manufacturing and selling textiles, but can only be used for samples with a uniform color. Many textiles are polychromatic with complex variegated patterns. Microscopy is useful in the analysis of single textile fibers [6], but the colorimetry of single textile fibers is difficult because many light microscopes use transmitted light from a tungsten source, whereas textile color is usually measured relative to daylight reflectance. White

light-emitting diodes in many modern microscopes add an extra layer of complexity, because their emission spectra have three peaks corresponding to RGB color vision. Even with a constant emission spectrum from a single illuminator, relationships between transmittance and reflectance are complicated by light scattering in the sample, as well as by the method of measurement.

When synthetic dyes, mordants and fiber chemistry are controlled in manufacturing textiles, microcolorimetry may be straightforward. A far greater challenge, however, is the deductive study of unknown samples, whether manufactured by a competitor or found in a museum collection, and where the replacement of natural dyes by synthetic dyes may have taken place [7]. Synthetic dyes offer many advantages industrially, but natural dyes continue to be used in traditional and art textiles. As example in this review, let us consider red colorants in Peruvian alpaca wool products, such as natural cochinitilla (rosada and rojo), now being replaced by synthetic dyes [8, 9].

Annatto prepared from the outer parts of seeds of *Bixa orellana* is widely used as a yellow colorant for butter and cheese, but can produce pink or red when used on cotton or silk. A particularly intense red hue is produced when annatto is painted on wood previously treated with white clay, as in an Amazonian zunidor (a flat paddle on a string rotated about the head of the user to produce a musical sound). The Pantone system (Pantone, 590 Commerce Blvd, Carlstadt, NJ) was chosen as a reference because it is widely used for textiles and the color chips could be measured by fiber-optics to interface with CIE values. Data were tested using a *t*-test at each wavelength. The reference colorant was carmine with certified standards for histological use.

3.1 Dye powders and solutions

A great advantage of microcolorimetry is that we can encompass the whole range from powdered colorants, to their solutions, to blots on a standard substrate like filter paper, and eventually to the target textile fibers. The differences between the colorimetry of dye powders and their solutions give us a good example of distributional error in spectrophotometry and, hence, colorimetry. Imagine measuring the transmittance of a uniformly dissolved dye in the cuvette of a spectrophotometer, then causing the dye to form a crystal by lowering the temperature. Light that was first subject to selective absorbance by the dissolved dye would then pass unaltered around the crystal, thus producing a profound change in the transmittance spectrum – even if the crystal was still in the optical axis. This is quite a classical problem in microscope spectrophotometry, although it can be corrected with a two-wavelength correction for distributional error, by comparing absorbencies at the maximum and minimum of the dye, or by scanning with a small aperture [3]. But with light reflected from dye powders there is also the problem of reflectance from crystal surfaces. Fiber-optic reflectance of dye powders showed that carmine had higher reflectance of red light than either cochinitilla rosada ($P < 0.001$ from 600 to 680 nm), or cochinitilla rojo ($P < 0.001$ from 590 to 700 nm). The reflectance spectra of carmine powder were similar in shape to that of cochinitilla rojo, which is to be expected because carmine is refined from cochinitilla rojo. Thus, their CIE chromaticity coordinates were very similar ($x = 0.674$ and $y = 0.295$ for carmine, and $x = 0.669$ and $y = 0.297$ for cochinitilla rojo) although carmine had a high luminosity ($Y\% = 1.85$) while cochinitilla rojo had a relatively low luminosity ($Y\% = 0.53$), although this may have been influenced by the small particle size and light scattering from a mordant in the refined carmine stain. The spectrum for cochinitilla rosada has a higher reflectance of blue-green light than either carmine ($P < 0.001$ from 450 to 680 nm, and $P < 0.05$ at 590 and 690 nm) or cochinitilla rojo ($P < 0.001$ from 400 to 600 nm and $P < 0.05$ at 610 nm). Thus, the relatively high blue-green reflectance of cochinitilla rosada reduced chromaticity coordinate x to 0.419 (towards blue in the CIE diagram) without much change towards yellow ($y = 0.388$). Details of blue-green reflectance were difficult to see in the overlapping lines, which is why they are shown logarithmically as absorbance values in Figure 2. In the Pantone chart, carmine \approx 181761, cochinitilla rojo \approx 191860, and cochinitilla rosada \approx 191625.

Transmittance of red light through dye solutions (all at equal weight by volume concentration) showed that carmine had stronger absorbance than cochinitilla rojo ($P < 0.01$ from 570 to 680 nm) or cochinitilla rosada ($P < 0.001$ from 560 to 700 nm). Carmine had a secondary transmittance peak at 420 nm and cochinitilla rosada had a secondary peak at 450 nm, but no secondary violet or blue peak was found for cochinitilla rojo (transmittance \approx 0). Wavelength separation of secondary peaks was significant, $P < 0.01$. The hue of cochinitilla rosada solution ($x = 0.527$ and $y = 0.210$) was very similar to the classic hue of carmine solution ($x = 0.542$ and $y = 0.212$), whereas cochinitilla rojo solution was more orange ($x = 0.687$ and $y = 0.313$).

3.2 Blots

Drops of stain solution were used to make circular blots on filter paper which then were measured by fiber-optics after drying. Measurements were made at the centers of blots. Staining intensity was low for carmine blots and they had higher reflectance than for cochinitilla rojo (Figure 3; $P < 0.001$ from 400 to 700 nm) and cochinitilla rosada ($P < 0.001$ from 510 to 590 nm, and $P < 0.01$ from 620 to 700 nm). For carmine, note the low reflectance and dimple around 550 nm; a similar dimple for cochineal was shown by Saltzman [11], although it was around 520 nm and only observed in an absorbance spectrum and, strangely, did not show in a reflectance spectrum. Blots for cochinitilla rojo had a lower reflectance of violet and blue than either carmine or cochinitilla rosada ($P < 0.001$ from 400 to 540 nm). Blots for cochinitilla rosada ($x = 0.345$ and $y = 0.263$, Pantone \approx 172625) were similar in hue to blots for carmine ($x = 0.355$ and $y =$

0.301; Pantone \approx 163118), whereas blots for cochinitilla rojo appeared orange ($x = 0.423$ and $y = 0.315$; Pantone \approx 161641).

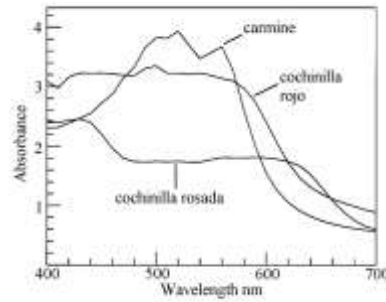


Figure 2. Three dye powders measured by fiber-optic reflectance, then converted to absorbance to separate the lines.

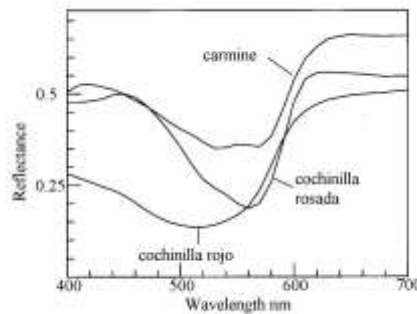


Figure 3. Fiber-optic reflectance spectra of three dye solutions blotted on filter paper.

3.3 Annatto

Annatto may contain a number of minor carotenoids in addition to the major colorants - bixin in liposoluble preparations and norbixin in hydrosoluble preparations. Fiber-optic reflectance showed the white background of the zunidor had an almost flat spectrum, sloped with a low at 400 nm and a high at 700 nm (Figure 4). This may have included a varnish to stabilize the white clay. The spectrum for annatto red from the berries of *Bixa orellana* showed a sharp cut-off centered at 600 nm. There was no trace of a secondary peak near that of solutions of carmine at 420 nm or cochinitilla rosada at 450 nm, or towards 400 nm for blots of carmine, cochinitilla rojo and rosada. For annatto red, $x = 0.503$ and $y = 0.348$, and Pantone \approx 181664.

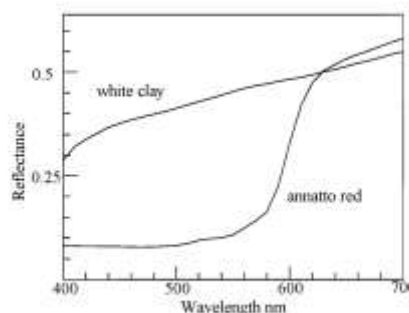


Figure 4. Fiber-optic reflectance spectra of annatto red on the white clay background of an Amazonian zunidor.

3.4 Alpaca wool

For microscope spectrophotometry, the main problem was penetration of the dye centripetally into wool fibers. For cochinitilla rosada and rojo, almost the full depth of the cortex was stained and was measurable with a large photometer aperture. But with a small aperture to measure the minimal penetration of carmine, there was refractive dispersion near the Beck line which made spectrophotometry unreliable for measuring dye absorbance. Spectra for cochinitilla rosada ($x =$

0.398 and $y = 0.347$) differed from cochinitilla rojo (Figure 5; $x = 0.334$ and $y = 0.261$) from 400 to 510 nm and from 540 to 590 nm ($P < 0.001$).

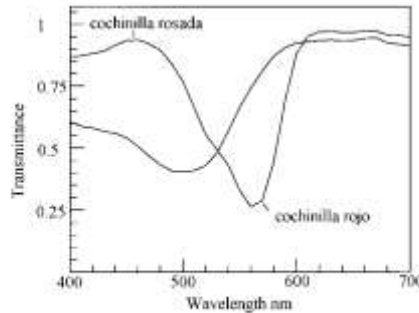


Figure 5. The cortex of alpaca wool fibers after staining, measured by microscope transmittance.

3.5 Scattering

The main problem in using reflectance and transmission data for colorimetry may be light scattering. For a solution with a uniformly distributed chromospheres in a cuvette, and for a known path length of collimated light, transmittance in its logarithmic form (absorbance) may be used directly to estimate chromophore concentration, but not if there is turbidity or distributional error (such as selective staining or chromophore precipitation) in the light path. Similarly, for colorimetry using microscopy or fiber optics, scattering may produce chromatic effects as a source of error. Scattering tends to be inversely proportional to a power of wavelength, which is why the spectra reported in this chapter were particularly variable towards 400 nm. Goniophotometry shows that scattered light is usually deflected from the primary optical axis of the measuring system to reappear off-axis.

Dry powders with limited light penetration had very low reflectance towards 400 nm, whereas clear dye solutions with no scattering had low transmittance at 400 nm but secondary peaks showing. Stained filter paper with high scattering had reflectance increased towards 400 nm, rather like dye on white clay which had medium scattering and reflectance increased towards 400 nm. Wool with high scattering had reflectance high at 400 nm, while single wool fibers with strong scattering had very high transmittance at 400 nm. Thus, differences in the scale and type of measurement (microscopy *versus* fiber optics, or transmittance *versus* reflectance) had only a minor effect on colorimetry, while scattering had a major effect. Testing this idea, differences in absolute values of transmittance and reflectance attributable to the scale of measurement were cancelled by taking a ratio, 400/700 nm. This ratio was strongly correlated with chromaticity coordinate x , $r = -0.86$, $P < 0.001$, $n = 18$, whereas no relationship of the 400/700 nm ratio with chromaticity coordinate y was detected ($r = -0.09$). This shows that light scattering from the subsurface of a sample is important for colorimetry, especially for translucent samples.

4. TEETH

Dental colorimetry is a major commercial industry mostly using subjective matching of color chips, but there are other aspects to tooth colorimetry. Tooth color in rodents is an interesting insight into how animals are adapted to their place in nature. How do beavers keep sharp teeth to chisel their way through substantial trees, dropping the trees into rivers for winter nourishment from the bark? The hardness of rodent teeth is a result of small amounts of iron and magnesium in the dental matrix [12], which produces the yellow-orange colors in many museum exhibits of rodent incisors. What about colorimetry? Hard anterior enamel (yellow-orange) and posterior softer enamel (white), become worn to keep a sharp edge from anterior hardness and posterior abrasion. Measured by fiber optics, an incisor tooth of a beaver (*Castor canadensis*, mandible) had the anterior yellow-orange part with $x = 0.54$, $y = 0.44$, $Y\% = 17.0$, while the posterior white part was $x = 0.35$, $y = 0.35$, $Y\% = 51.7$ (Figure 6).

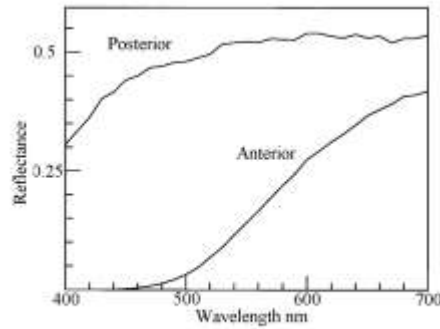


Figure 6. Fiber optic spectra from an incisor tooth of a beaver.

5. INTERFERENCE COLORS

Bright, metallic interference colors are a real challenge in colorimetry because they are more spectacular than pigment colors, which are usually modified by substrate scattering. The structural colors of insects [13] are quite distinct from those of plant pigments [14], with countless implications in predation and animal vision. There has not been much interest in interference colorimetry – measuring our perception of iridescence. White chalk illuminated with sunlight reflects a broad spectrum of wavelengths which our tristimulus color vision interprets as white. But a white area on a computer screen is really an area of three balanced pixel hues that have tricked our eyes to appear white; and when we perceive interference colors, complex interference spectra trick our eyes again. As the order of interference increases, the colors appear to change from metallic sheens to misty pastels, but the hues are repeated in a regular sequence. We are all familiar with iridescence on credit card holograms, stressed glass and oil slicks, but interference colors often tend to be sharply localized, and may require microscopy for their analysis.

A widely used subjective method of microscope colorimetry is for identifying thin sections of minerals, where the thickness of sectioned mineral must be known accurately [15]. The interference color produced by the path difference between ordinary and extraordinary rays in a polarizing microscope is compared subjectively with the colors on a Michel-Lévy color chart, named after French geologist Auguste Michel-Lévy (1844-1911). The grid lines on the chart identify minerals by their birefringence relative to section thickness.

Interference colors typically show a series of sinusoidal waves which interact with the spectral sensitivities of the human eye to create sensations of various hues, whereas a Michel-Lévy color chart uses colorants to simulate the hues of interference colors. There is considerable variability in the success of printers to simulate interference colors using pigments [16], and charts may fade. Here we will consider how real interference colors compare with colorants on a chart (Figure 7).

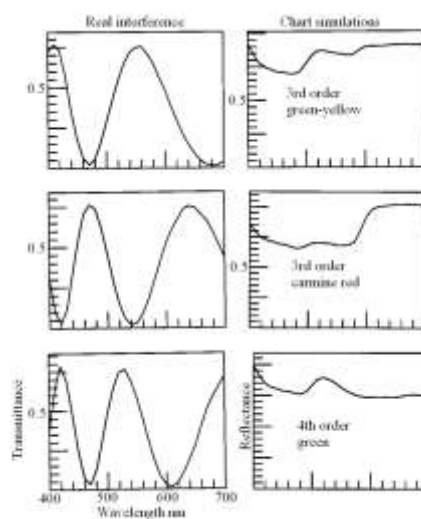


Figure 7. Real interference colors created by a tilting compensator in a polarizing microscope compared with fiber-optic reflectance spectra of a Michel-Lévy color chart from Zeiss.

6. IRIDESCENCE FROM DIFFRACTION VERSUS MULTILAYER INTERFERENCE

Iridescent blue barbules of a feather from a blue peacock (*Pavo cristatus*) were trimmed to fit into a well slide (tube depth 2.5 mm, inner diameter 13 mm). For measurements under water, the meniscus was adjusted to avoid a flat surface in the optical axis. A trace of detergent was added to the water to overcome preen oil preventing surface wetting. Diffractive iridescence on the peacock feather (Figure 8) had a single major peak at 520 nm and the start of harmonics at higher wavelengths, which is why in optical apparatus a diffraction grating monochromator requires filters to remove stray light (Figure 1). Wetting caused major changes ($P < 0.001$) in reflectance from 450 to 690 nm associated with major changes in chromaticity coordinates (x from 0.231 ± 0.006 to 0.246 ± 0.003 , $P < 0.01$; y from 0.366 ± 0.016 to 0.238 ± 0.005 , $P < 0.001$; and $Y\%$ from 53.96 ± 5.33 to 14.42 ± 0.34 , $P < 0.001$). The change in $Y\%$ shows very clearly, as discovered by Hooke in 1665 [2], that the wet feather was much darker than the dry feather.

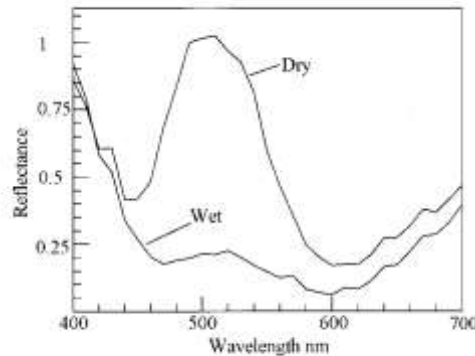


Figure 8. Iridescent blue on barbules of a peacock feather extinguished by wetting.

The nacre of a dark pearl button (*Pinctada margaritifera*) with strong iridescence was measured dry and wet. Iridescence from multilayer interference in the nacre (Figure 9) was quite different to feather iridescence and had two peaks, at 460 nm and 620 nm, originating from the two primary layers in this example. At places where other iridescent hues were visible, the peaks were shifted across the spectrum. In contrast to the iridescence of the peacock feather, the iridescences of nacre showed no meaningful changes under water.

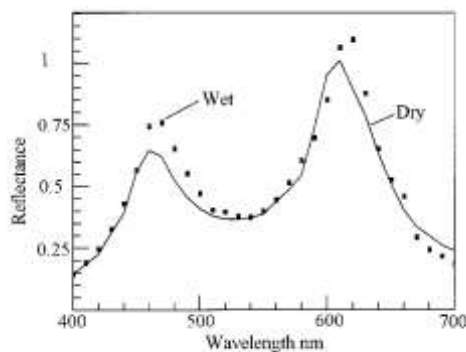


Figure 9. Multilayer pink iridescence of pearl nacre unaffected by wetting.

7. IRIDESCENCE IN MEAT

Meat colorimetry is relatively simple. The muscles from which meat is derived contain a mixture of fibers, specialized either for aerobic metabolism (high myoglobin) or anaerobic metabolism (low myoglobin). Myoglobin is bright red when carrying oxygen, purple when deprived of oxygen, or brown when the myoglobin is oxidized. But the real challenge is understanding meat iridescence. Green iridescence on meat or fish muscle displayed for sale in a supermarket often gets consumers concerned [18, 19]. The iridescent colors of meat look very much like interference colors, but what causes the interference? The dominant explanation on the internet at the present time is that iridescence is caused by surface diffraction from myofibrillar serrations [20], with no explanation of how soft myofibrillar serrations can still act as diffraction gratings when tightly compressed by a packaging film. As discovered by Hooke in 1665 [2], and confirmed in this review (Figure 8), the strong iridescent colors of peacock feathers caused by surface diffraction

disappear when a feather is placed under water, and there is no reason to doubt this because replacing the negligible refractive index of air with the substantial refractive index of water should change dispersion at a grating surface. Hence, a critical test of the diffraction hypothesis of meat iridescence – does iridescence disappear when meat is submerged under water?

An alternative explanation to diffraction causing meat iridescence is multilayer interference [21, 22]. Sarcomere discs may reflect incident light at refractive index boundaries (A-band > I-band), light reflected from lower discs will have a longer light path than light reflected from upper discs, so that light waves following long light paths will often be out of phase with waves following short paths. But when living muscle is converted to meat, the development of *rigor mortis* may vary from fiber to fiber. The first fibers to deplete their adenosine triphosphate usually contract, which throws other fibers into sinuous folds [23] so that their A bands lose the alignment normally maintained by the cytoskeleton [24, 25]. Thus, iridescence is a sporadic phenomenon dependent on the complex situation as *rigor mortis* develops. A sirloin from a Canadian whitetail deer (*Odocoileus virginianus*) obtained by hunting was roasted to a well done state (perimysium gelatinized) and 2-mm sections of *gluteus medius* were cut across the grain with a scalpel blade. Sarcomere length determined by microscopy was $1.45 \pm 0.14 \mu\text{m}$, $n = 100$.

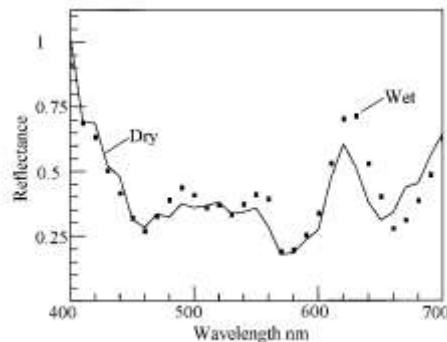


Figure 10. Orange iridescence in muscle fibers of roast venison unaffected by wetting.

Orange iridescence in muscle fibers of roast venison (Figure 10) was like the multilayer spectrum of nacre (Figure 9) in having peaks from several reflective layers, most likely A bands. An important point is that the iridescences of both nacre and venison were maintained under water, whereas the diffractive iridescence of the peacock feather was largely extinguished. Hence it was concluded that iridescence in roast venison originated from multilayer interference and not from surface diffraction. What about the effect of cooking? Apart from surface browning, the major change in the interior of a roast is coagulation of sarcoplasmic proteins, much as egg albumen becomes opaque and white when heated. This causes a massive increase in $Y\%$, but the A and I bands responsible for multilayer reflective interference retain their birefringence and show little change [26].

In Figure 10, the reflectance of violet light at 400 nm was high because light scattering in meat is a function of wavelength, such that light at 400 nm is highly scattered back to the illuminated surface, while red light at 700 nm tends to penetrate deeply into the meat and becomes trapped [27]. Hence, with transmitted light, transmittance through meat is low at 400 nm while transmittance at 700 nm is high. But with reflected light, as measured here, reflectance at 400 nm was high because of high scattering

It is possible that interference from A band reflectance is a major cause of light scattering along muscle fibers, remembering that meat is optically anisotropic with different properties along versus across muscle fibers detectable by goniophotometry [27]. Interference along fibers may explain why reflectance is sometimes correlated with sarcomere length [28]. Thus, iridescence may be a special case of light scattering in the long axis of muscle fibers. The practical importance of longitudinal scattering is that it may frustrate attempts to predict meat tenderness from optical measurements. On one hand, low pH may increase light scattering in tender meat while, on the other hand, short sarcomeres in tough meat may also increase light scattering. In samples with a similar pH, high scattering from short sarcomeres may predict toughness, but in samples with similar sarcomere lengths low scattering may predict toughness. Dealing with optical anisotropy in meat may be the key to making optical predictions of meat toughness more reliable in samples with a range in both pH and sarcomere length.

8. BOOLEAN ANALYSIS OF SPECTRA

A variety of optical probes are used in the meat industry, with one of the main applications being to measure the depth of fat on the back of a pork carcass. Canadian pork producers are paid for producing lean meat, so a carcass with a shallow depth of subcutaneous fat is worth more than a carcass of the same weight which is very fat. The change in reflectance as a probe passes from fat to connective tissue on the muscle surface is fairly easy to identify with a broad-band reflectance

measurement, but some pigs have very pale meat – a phenomenon known as the pale, soft, and exudative (PSE) condition which must be detected when assembling a shipment at a premium price. Fiber-optic reflectance spectra provide a solution to this problem, which does not require accurate colorimetry, but does require a fast decision made in a learning context to compensate for drifting emission spectra and photometers. Probability matrices were used to distinguish between the PSE muscle and surface connective tissue as follows.

The reflectance (R) spectrum from wavelength (λ) 1 to n was converted to a probability matrix (Pmat). For R from λ 1 to n, the Pmat was visualised as a triangular matrix containing $(n * (n-1)) / 2$ scalars used to store a comparison of R at each λ compared with R at all other λ . Column 1 of a Pmat contained the results of comparing R at λ 1 with R at λ 2 to n, column 2 of Pmat contains the results for λ 3 to n, etc. If R at one λ was less than R at another λ , a value of -1 was assigned to the appropriate position in Pmat. Conversely, if R at one λ was greater than R at another λ , a value of 1 was assigned to the appropriate position in Pmat. With numerous decimal places derived from analogue to digital conversion of the photometric signal, very rarely (if ever) was R at one λ exactly equal to R at another λ . This triangular matrix is to explain and display the method of operation here – in practice, a vector was used to simplify the software.

For each type of tissue, a cumulative probability matrix (Cpmat) was trained by adding the Pmats of known spectra. The scalars in a Cpmat were called accumulators. Thus, the accumulators in a Cpmat became more negative if R at a particular λ consistently was less than R at another λ , while the accumulators became more positive if R at a particular λ consistently was higher than R at another λ . However, accumulators for comparisons with a random outcome tended to zero. After a Cpmat was trained, the accumulators were divided by the number of spectra used for training. Thus, the maximum range for any accumulator in a completed Cpmat was from -1 to 1.

Cpmats from different tissues exhibited many similarities (as may be seen by comparing the Cpmats for CT and PSE in Figure 11). For example, reflectance in the Soret band (column 2 for the matrices shown in Figure 11) generally was low in all spectra, because most contained traces of hemoprotein, either from myoglobin in muscle or residual hemoglobin in connective tissue. Thus, Cpmats did not allow reliable deductions to be made about unknown spectra. But reliability was greatly increased by subtracting the Cpmat of one tissue from the Cpmat of another tissue to create a matrix of differences in cumulative probabilities (Dcpmat). The scalars in a Dcpmat were called weightings. For example, if equivalent accumulators in Cpmats for non-muscle and muscle both had a value of 1, then subtraction of one Cpmat from the other cancelled the weighting of this accumulator ($1 - 1 = 0$). Thus, features common to both matrices were cancelled and their weightings approached zero, while dissimilar features were enhanced to give stronger weightings as follows: $1 - (-1) = 2$, and $(-1) - 1 = -2$.

A Pmat for a single unknown spectrum collected from a carcass by a robot navigating to the measuring position from ultrasonic scans of the skeleton was evaluated as follows. The Pmat of the unknown spectrum was multiplied by the Dcpmat for muscle minus non-muscle. The scalars of the Pmat were either -1 or 1 (rarely 0). The weightings of the Dcpmat ranged from -2 to 2. If the scalar and the weighting were both negative then the product was positive, for example, $-1 * -2 = 2$. Similarly, if the scalar and the weighting were both positive then the product was positive, for example, $1 * 2 = 2$. But the products were negative if the scalar and weighting differed in sign, for example, $1 * -2 = -2$. Thus, the sum of Pmat scalars multiplied by Dcpmat weightings (S_{muscle}) gave a measure of the number and importance of similarities between the unknown Pmat and the Dcpmat, with non-matching features being subtracted from matching features. This operation was repeated for the inverse case where the Dcpmat was derived by subtracting a muscle Cpmat from a non-muscle Cpmat. Thus, the final probability for an unknown spectrum originating from muscle was $S_{\text{muscle}} / (S_{\text{muscle}} + S_{\text{non-muscle}})$.

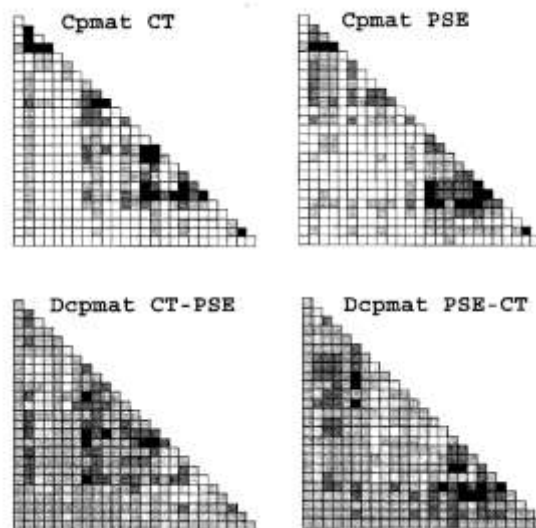


Figure 11. LaserJet pixel patterns used to display pseudogray maps of triangular matrices used in learning to distinguish between white connective tissue (CT) and very pale pork muscle (PSE). Matrices were scaled from 0 to 1. For 0, no LaserJet

pixels were activated in a grid box corresponding to matrix rows and columns; for 0.5, half of the pixels were activated; and for 1, all the pixels were activated to give a solid black grid box. In cumulative probability matrices (Cpmat) and differences in cumulative probability matrices (Dcpmat), darkness indicates a low value and lightness indicates a high value. Column 1 (left) row 1 (top of column) compares 400 with 410 nm, column 1 row 2 compares 400 with 420 nm, and so on down the column. Column 2 row 2 (top of column) compares 410 with 420 nm, column 2 row 3 compares 410 with 430 nm, and so on down the column. The single row of the last column (right) compares 640 with 650 nm.

The system was standardized by learning on static samples, and as few as three spectra gave a matrix against which unknown spectra could be compared with reasonable success (87% correct). Thus, when moving through a pork carcass, it was possible to detect the boundary connective tissue and correct location of the probe within a muscle. Unfortunately, the robotic system did not become commercially viable; mainly because of the engineering problem in bringing a moving carcass to a complete standstill fast enough to keep up with commercial line speeds, but the ultrasonic navigation system and Boolean colorimetry showed great promise and may yet find an easier application in the food industry [29]. For example, beef is extremely tough the day after slaughter and requires several days aging for a cheap product, and many weeks aging for a premium product. Spectrofluorometry with a photodiode array giving almost instantaneous spectra can detect the subtle changes in connective tissue occurring as beef is aged [30].

9. DISCUSSION

Spectrum analysis has a long history, from Newton and Hooke in the 1600s, through Fraunhofer and Lockyer in the 1800s [31], and there is no doubt that spectrum analysis has contributed greatly to our contemporary understanding of natural phenomena – from astronomy, to the discovery of chemical elements, and to understanding biologically important molecules. The application of spectrum analysis to art and industry also has a long history [32]. With colorimetry we may sacrifice a vast amount of information, reducing full spectra to a few chromaticity coordinates, but we establish an interface with human color vision. This is of paramount importance in countless aspects of engineering and technology where products are produced for human appreciation and consumption. The age of machine vision may be upon us, but the human eye still commands great power, whether in choosing to purchase manufactured goods or strolling through an art gallery.

Microscope spectrophotometry also has a long history, with conventional methods using prism and grating monochromators combined with photomultipliers reaching a high level of proficiency in the 1970s. Many microscope spectrophotometers are now commercially available, but their main problem is proprietary software that excludes the researcher who would attempt something unusual or original. Thus, a simple microscope spectrophotometer is most useful if speed of measurement is not critical. If there are no time constraints, there is time for a spectrophotometer with a prism, grating, or continuous interference filter to step through the required spectrum – easy to standardize and easy to program [3]. With time constraints, to avoid fluorescence bleaching [30] or to navigate a robotic probe [29], a photodiode array justifies the investment in software, and this is doubtless the direction that instrument manufacturers will take, selling systems that require little user understanding and always making the same measurements. But a key feature in scientific progress is the scientist's ability to make new apparatus to make new measurements so, for those on a limited budget, there will always be a premium for a relatively simple system to modify.

Having segregated potential users for microcolorimetry into low-budget innovators versus well-funded technician teams making routine measurements, the next question is the working environment. Industrial environments are seldom easy places to use complex apparatus. From the food factory to the machine shop, we may have to cope with extremes of temperature, vibration, humidity, corrosion, static electricity, power surges, and operator error. From experience as a low-budget innovator, the best solution has been to locate a microphotometer in a safe room and to link it to the working environment using optical fibers and low-voltage data cables. The operator in the working environment then needs nothing more than push-button switches and display lights to control the system – not forgetting controls to enter sample identification codes and being able to retreat in the measuring process and to delete last-stored erroneous data. For manufacturers of equipment for routine measurements, the other option might be to miniaturize everything with a radio link to a server.

Whatever route we may take, there is the problem of standardization. In macroscopic colorimetry there is a hierarchy of white standards from new magnesium oxide, to barium sulfate powder pressed in a standardized manner, to opal glass plates – with everything relatable back to magnesium oxide. But how can we use this with a microscope (that easily detects highly reflective crystal surfaces) or fiber-optics (where optical fiber numerical aperture and linkage to the standard have major effects)? For low-budget innovators a solution is to use Teflon. Teflon tape may be slightly different from the pressed powder used in macroscopic colorimetry [4], but several layers of tape can be used both around a microscope slide and in the aperture of a fiber-optic system (remembering the microscope has a collimated illumination while a bare optical fiber does not – hence the importance of the back-off distance and the refractive index of the medium linking the optical fiber to the standard). Might there be errors in microcolorimetry caused by using several layers of Teflon tape as a white standard?

10. REFERENCES

- [1] Billmeyer, F.W., Saltzman, M. (1981). *Principles of Color Technology*. John Wiley & Sons, New York. 240 pp.

- [2] Hooke, R. (1665). *Micrographia or Some Physiological Descriptions of Minute Bodies Made by Magnifying Glasses with Observations and Inquiries thereupon*. Royal Society, London. Facsimile reproduction, 1961, Dover Publications, New York, p. 168.
- [3] Swatland, H.J. (1998). *Computer Operation for Microscope Photometry*. CRC Press, Boca Raton, FL. 238 pp.
- [4] Weidner, V.R., Hsia, J.J. (1981). Reflectance properties of pressed polytetrafluoroethylene powder. *J. Optic. Soc. Amer.* 71: 856-861. <http://hep.ucsb.edu/people/hnn/n/nbspfte.pdf>
- [5] Swatland, H.J. (1991). Effect of refractive index and cutting angle on internal Fresnel reflectance at the distal window of an optical fiber. *J. Comput. Assist. Microsc.* 3:233-236.
- [6] Greaves, P.H. , Saville, B.P.(1995). *Microscopy of Textile Fibres*. Royal Microscopical Society, Microscopy Handbooks 32. Bios Scientific Publishers, Oxford. 92 pp.
- [7] Ferreira, E.S.B., Hulme, A.N., McNab, H., Quye, A. (2004). The natural constituents of historical textile dyes. *Chem. Soc. Rev.* 33: 329-336. <http://pubs.rsc.org/en/content/articlelanding/2004/cs/b305697j#!divAbstract>
- [8] Antúnez de Mayolo, K.K. (1989). Peruvian natural dye plants. *Econ. Bot.* 43: 181-191. <https://link.springer.com/article/10.1007/BF02859858>
- [9] Fischer, C.H., Rabe, J.G., Bischof, M. (1990). Identification of natural and early synthetic textile dyes with HPLC and UV/vis-spectroscopy by diode array detection. *J. Liq. Chromatogr.* 13: 319-331. <http://www.tandfonline.com/doi/abs/10.1080/01483919008049546?needAccess=true&journalCode=jljlc19>
- [10] Dapson, R. W. (2007). The history, chemistry and modes of action of carmine and related dyes. *Biotech. Histochem.* 82: 173-187. <http://www.tandfonline.com/doi/abs/10.1080/10520290701704188?src=recsys&journalCode=ibih20>
- [11] Saltzman M. (1992). Identifying dyes in textiles. *Amer. Sci.* 80: 474-481. <http://www.jstor.org/stable/29774728>
- [12] Gordon, L.M., Cohen, M.J., MacRenaris, K.W., Joester, D. (2015). Dental materials. Amorphous intergranular phases control the properties of rodent tooth enamel. *Science* 347(6223):746-750. <http://science.sciencemag.org/content/347/6223/746>
- [13] Berthier S. (2007). *Iridescences. The Physical Colors of Insects*. Springer Science + Business Media: New York; 2007. 160 pp.
- [14] Lee, D. (2007). *Nature's Palette. The Science of Plant Color*. University of Chicago Press, Chicago. 409 pp.
- [15] Hurlbut, C. (1971). *Dana's Manual of Mineralogy*. John Wiley & Sons, New York. 579 pp.
- [16] Delly, J.G. (2003). The Michel-Lévy interference color chart – microscopy's magical color key. *Modern Microsc. J.*, July 10. <http://www.timeanddate.com/worldclock/city.html?n=1178>
- [17] Judd, D.B. (1952). *Color in Business Science and Industry*. John Wiley and Sons: New York. 401 pp.
- [18] Kukowski, A.C., Wulf, D.M., Shanks, B.C., Page, J.K., Maddock, R.J. (2004). Factors associated with surface iridescence in fresh beef. *Meat Sci.* 66: 889-893. <http://www.sciencedirect.com/science/article/pii/S0309174003002328>
- [19] Lawrence, T.E., Hunt, M.C., Kropf, D.H. (2002). Surface roughening of precooked, cured beef round muscles reduced iridescence. *J. Muscle Foods* 13, 68-73. <http://onlinelibrary.wiley.com/doi/10.1111/j.1745-4573.2002.tb00321.x/abstract>
- [20] Martinez-Hurtado, J.L., Akram, M.H., Yetisen, A.K. (2013). Iridescence in meat caused by surface gratings. *Foods* 2: 499-506. <http://www.oalib.com/paper/3095935#.Wd7AyvkrLDc>
- [21] Rayleigh, Lord. (1923). Studies of iridescent colour and the structure producing it. III. The colours of Labrador feldspar. *Proc. Roy. Soc., London. Series A*, 103: 34-45. <http://rspa.royalsocietypublishing.org/content/103/720/34>
- [22] Raman, C.V., Jayaraman, A. (1950). The structure of labradorite and the origin of its iridescence. *Proc. Indian Acad. Sci.* A32: 1-16. <https://link.springer.com/article/10.1007/BF03172469?no-access=true>
- [23] Bendall, J.R. (1973). Postmortem changes in muscle. In: *The Structure and Function of Muscle*. G.H. Bourne (ed.). Vol. 2, Part 2. 2nd edition. Academic Press, New York.
- [24] Pierobon-Bormioli, S. (1981). Transverse sarcomere filamentous systems: 'Z- and M-cables'. *J. Muscle Res. Cell Motil.* 2: 401-413. <https://link.springer.com/article/10.1007/BF00711967?no-access=true>
- [25] Wang, K., Ramirez-Mitchell, R. (1983). A network of transverse and longitudinal intermediate filaments is associated with sarcomeres of adult vertebrate skeletal muscle. *J. Cell Biol.* 96: 562-570. <https://www.ncbi.nlm.nih.gov/pubmed/6682107>
- [26] Aronson, J.F. (1966). A melting point for the birefringent component of muscle. *J. Cell Biol.* 30: 453-464. <https://www.ncbi.nlm.nih.gov/pubmed/5339378>

- [27] Swatland, H.J. (1988). Measurement of light scattering in normal pork using a fiber-optic goniophotometer. *J. Anim. Sci.* 66: 2578-2582. <https://www.animalsciencepublications.org/publications/jas/abstracts/66/10/JAN0660102578>
- [28] Swatland, H.J. (2003). Fiber-optic spectrophotometry of beef relative to sarcomere length. *Archiv. Anim. Breeding* 46: 31-34. <http://www.archanimbreed.com/pdf/2003/at03p031.pdf>
- [29] Swatland, H.J., Ananthanarayanan, S.P., Goldenberg, A.A. (1994). A review of probes and robots. Implementing new technologies in meat evaluation. *J. Anim. Sci.* 72: 1475-1486. <https://www.animalsciencepublications.org/publications/jas/abstracts/72/6/1475>
- [30] Swatland, H.J. (1995). Microscope spectrofluorometry of bovine connective tissue using a photodiode array. *J. Comput. Assist. Microsc.* 7: 165-170.
- [31] Lockyer, J.N. (1883). *Studies in Spectrum Analysis*. Kegan Paul, Trench & Co. London., 258 pp.
- [32] Rood, O.N. (1883). *Modern Chromatics with Applications to Art and Industry*. 2nd edition. Kegan Paul, Trench & Co., London. 330 pp.